Marine Multiple Attenuation Based on the See Floor Topography

Raimundo N. C. Carneiro*, Lourenildo W. B. Leite and Wildney W. S. Vieira, UFOPA*,UFPA, Brazil

Abstract

The present work aimed at a classical and continuous problem of multiple prediction and attenuation relating the multipaths between the free surface and ocean bottom topography.

The real seismic data analyzed covered from shallow to deep water levels, and the imaging was oriented to geological interpretation focused on oil exploration. The prediction model takes into consideration the information from the minimum common offset sections to delineate the sea floor, admitting low angles for the continental platform.

Once the multiple prediction has been well constructed, the time sections were NMO corrected, and geometrical spreading applied. After the basic processing, a Wiener-Hopf filter designed and optimally applied for the predictive attenuation.

Comparison of the results and methodology is to be made with other free marine surface multiple attenuation.

Introduction

One of the first processing challenges to improve the seismic section quality continues to be multiple attenuation. And the main reason is that most theories take into account only the primary reflections.

In the other hand, several theories take into account the presence of multiple for modeling and imaging. In shallow seismic (and side scan sonar) data, the presence of free surface multiple can represent the major visual of the section. Therefore, attenuation or make-use of multiples can be welcome complementary methodologies for the imaging.

In our context, the fundamental part is the estimation of the multiple path along the seismic profile (prediction, picking), that makes simpler its visualization and interpretation with respect to the sea floor topography.

The area for interest in marine oil exploration is limited to the continental platform, that usually shows a smooth topography (much less than five degrees slope angle).

The general minimum offset section has its normal incidence rather close to the geological Cartesian vertical axis. For a real vertical spatial propagation, the observation time axis of the image differs from the vertical spatial axis for a scale function factor. We have performed a Kirchhoff migration focusing on the water/basement contact to estimate the difference with respect to the minimum offset information, but this added process showed no to improve the details of its topography.

The main objective here is to couple a prediction-attenuation model based (geometry and physical parameters) process, with the result analyzed by comparison between the input and the output. The data is described as a random process, and the Wiener-Hopf operator is designed by taking into account a probabilistic distribution for the error difference between the desired and real output (Mesko (1984)). The efforts were not only around the filter theory, but first in the prediction strategy.

The infinite possibilities to describe multiple paths are constrained to the amplitude variation due to the reflection and transmission coefficients; that is, these internal coefficients are rather small, as a result the multiple paths have amplitudes small enough to be under the local noise amplitudes. Even thou, the multiple as a noise component can still have a meaningful correlation pattern.

A strategy was followed in this work, and resumed as:

1. Pre-processing for geometry, trace quality control, and gains,
2. Spherical divergence correction,
3. Picking of the free surface multiple on minimum offset sections,
4. Organization of CMP families,
5. NMO correction,
6. Application of the WH predictive deconvolution filter,
7. Time migration,
8. Time axis rescaling,
9. Velocity transformation,
10. Depth migration.

Methodology

Wiener-Hopf Filtering

A seismogram results from a field experiment, and contains all possible information about the unknown subsurface (medium). Also, strictly speaking the source (input) is unknown. These conditions sets up an inversion (deconvolution) problem where only the output (seismogram) is known, and we classify it as a blind inversion process. Therefore, to develop a practical technology for such an important aim, it is needed a priori information and constraints to build a convenient deconvolution operator (Peacook and Treitel (1969); Robinson and Treitel (1969); Robinson (1984); Makhoul (1978); Berkhout and Zaanen (1979)).

The filter coefficients are obtained from the solution to an optimization problem in the least-square sense, where the object function is given by the expectation of the distribution of errors, $e(h_j)$, between desired, z_k, and real, y_k, outputs:

$$e(h_j) = E\left\{(z_k - y_k)^2\right\}, \tag{1}$$

to be minimized as function of the h_j coefficients. This means to search for the minimum variance, as $E\{(z_k - y_k)\} = 0$. The filter output, y_k, is given by the convolution between h_k and the observed input g_k as:

$$y_k = \sum_{i=0}^{P-1} h_i g_{k-i}, \qquad (k = 0,1,2,...,N-1, \Delta t = 1). \tag{2}$$

It is admitted that the theorectical $E\{.\}$ makes the randomness non existent. As a consequence, the function $e(h_j)$ is non random, and the the relation to deterministic processes are equivalent as for differential and integral calculus (Makhoul (1978)). For the minimization, the criteria is that the partial derivatives with respect to the h_j coefficients be null, what means that the the searched point in parameter space is close to the solution, i.e.: $\frac{\partial e(h_j)}{\partial h_j} = 0$. The partial derivative operation results in the normal linear WH equation:

$$\sum_{i=0}^{P-1} h_i \phi_{gg}(j-i) = \phi_{zg}(j), \quad (j = 0,1,2,...,P-1). \tag{3}$$

The quantity $\phi_{gg}(j-i)$ is the autocorrelation of the input g_k. The $\phi_{zg}(i)$ is the unilateral positive part of the theorectical crosscorrelation between the desired output, z_k, and the real output, z_k.

The principle applied to construct the WH equation allows for several practical operations, but we restrict to the so called Predictive Operator. The matrix structure corresponding to equations (3) has the form:

$$\begin{pmatrix} A_{00} & A_{01} & \cdots & A_{0,P-1} \\ A_{10} & A_{11} & \cdots & A_{1,P-1} \\ \vdots & \vdots & \vdots & \vdots \\ A_{P-1,0} & A_{P-1,1} & \cdots & A_{P-1,P-1} \end{pmatrix} \begin{pmatrix} h_0 \\ h_1 \\ \vdots \\ h_{P-1} \end{pmatrix} = \begin{pmatrix} c_0 \\ c_1 \\ \vdots \\ c_{P-1} \end{pmatrix} \tag{4}$$

where $A_{ij} = \phi_{gg}(j-i)$, $c_j = \phi_{zg}(j)$.

Predictive WH Deconvolution

In the present model the desired output is $z_k = g_{k+T}$. Therefore, z_k is a prediction of g_k at a time distance T, in this way we have:

$$\begin{pmatrix} A_{00} & A_{01} & \cdots & A_{0,P-1} \\ A_{10} & A_{11} & \cdots & A_{1,P-1} \\ \vdots & \vdots & \vdots & \vdots \\ A_{P-1,0} & A_{P-1,1} & \cdots & A_{P-1,P-1} \end{pmatrix} \begin{pmatrix} h_0 \\ h_1 \\ \vdots \\ h_{P-1} \end{pmatrix} = \begin{pmatrix} A_T \\ A_{T+1} \\ \vdots \\ A_{T+P-1} \end{pmatrix} \tag{5}$$

where h_k is called prediction error operator, and h_k^* is the prediction operator defined by:

$$h^* = [1, \overbrace{0,0,...,0,0}^{(T-1)\text{zeros}}, -h_0, -h_1, -h_2, ..., -h_{N-1}]. \tag{6}$$

Normal Multiple Tracing

The objective is to attenuate the free surface multiple, by applying the WH method following the presented strategy. Therefore, the first step is to trace the multiple to define the periodicity T parameter, and for this it is necessary a model for the traveltime. For this case the water layer velocity (v_0) and geometry (angle α and segment position) is previously known, and the configuration for the modeling is as shown in Figure 1, that shows the sea floor approximated by linear segments. For this dipping topographical model, the multiples can be Normal or Oblique (Olhovich (1959)).

This strategy was implemented by Carneiro (2012), where the normal trajectory between sensor (at the marine free surface normal multiples) and the vertical to the sea floor (approximated by the minimum offset information) is given by equation (7):

$$t_n(x=0;k,\alpha) = (2k)\frac{h}{v_0 \text{sen}\alpha}\text{sen}(n+1)\alpha, \tag{7}$$

where n is the number of reverberations, k is the multiple order, α is the reflector topographical dip, and h the vertical thickness. The Normal multiples repeat themselves in a reverberation process (between source and receptor points), but the oblique do not repeat and propagate toward the deeper ocean.

Figure 1: Division of the continental platform in segments for the line Camamu 5519.

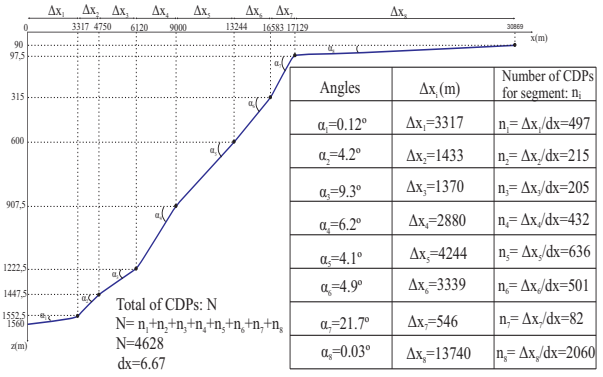

Angles	Δx_i(m)	Number of CDPs for segment: n_i
α_1=0.12°	Δx_1=3317	$n_1 = \Delta x_1/dx$=497
α_2=4.2°	Δx_2=1433	$n_2 = \Delta x_2/dx$=215
α_3=9.3°	Δx_3=1370	$n_3 = \Delta x_3/dx$=205
α_4=6.2°	Δx_4=2880	$n_4 = \Delta x_4/dx$=432
α_5=4.1°	Δx_5=4244	$n_5 = \Delta x_5/dx$=636
α_6=4.9°	Δx_6=3339	$n_6 = \Delta x_6/dx$=501
α_7=21.7°	Δx_7=546	$n_7 = \Delta x_7/dx$=82
α_8=0.03°	Δx_8=13740	$n_8 = \Delta x_8/dx$=2060

The calculated traveltimes were plotted over the common-offset section as shows Figure 2.

For comparison, in the case of oblique incidence down continental dip, the multiple does not present reverberation; i.e., it does not repeat between the source and receptor points, but repeats between the surfaces that constraints it. For x the distance source-receptor, the traveltime equation is given by:

$$t_n(x;\alpha,h) = \frac{1}{v_0}\sqrt{x^2 + \frac{4h}{\text{sen}\alpha}\left(\frac{h}{\text{sen}\alpha} + x\right)\text{sen}^2(n+1)\alpha}, \tag{8}$$

where α is the dip of a segment of the water layer topography bottom, as the continental platform, where the slope segment is very important in the marine case.

For some information, the Camamu seismic profile had the following parameters: (1) Number of shots: 1098; (2) Shot interval: 26.67m; (3) Number of receptors: 240; (4) Receptor interval: 13.33m; (5) Number of CMPs: 4628; (6) CMP interval: 6.67m; (7) Maximum fold: 60; (8) Rector

apertures: $300 - 3488$m; (9) Recording time: 4.5s; (10) Time sampling interval: 4ms.

The Camamu marine data was processed with the Seismic Unix (Cohen and Stockwell (2005); Forel et al. (2005)) format and programs. Figure 2 shows the tracing result, where the primary is in blue, and the first free surface multiple in green, and the second in red.

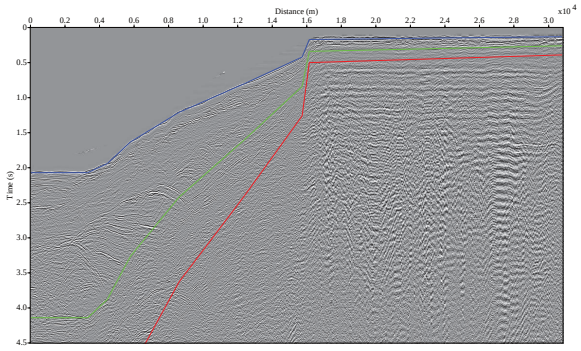

Figure 2: Minimum offset section from line Camamu 5519. The blue line corresponds to the tracing of the primary reflection, the green line to the first free surface multiple, the red line to the second and starts around 6.3s.

For the free surface multiple deconvolution we used the described strategy, by realizing the NMO correction to the CMP sections, according to there position in the profile, to have the periodicity in the multiple. Figure 3 shows the semblance velocity spectra for CMP 450, and figure 4 shows the correspondent CMP before and after the application of the NMO correction.

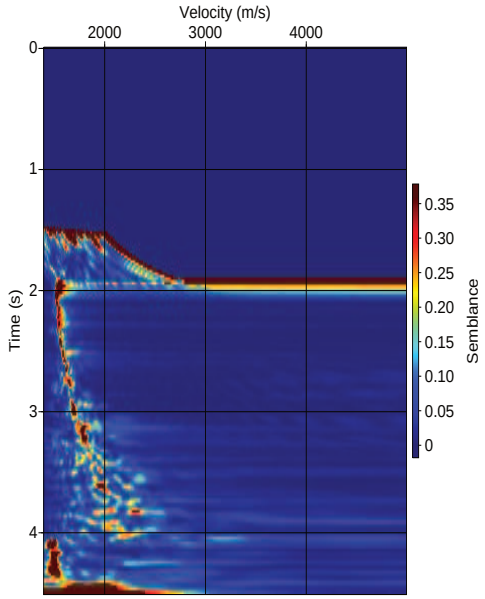

Figure 3: Semblance map for CMP 450.

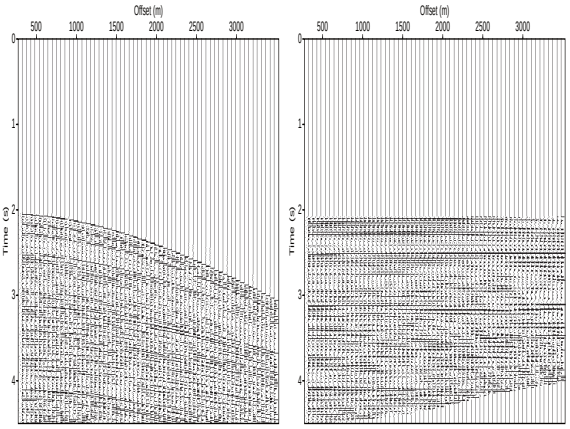

Figure 4: CMP 450 before (left), and after the NMO correction (right).

Figure 5 shows the NMO velocity distribution used for the stack.

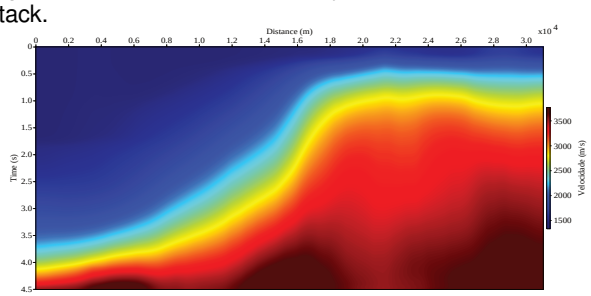

Figure 5: NMO smoothed velocity distribution. The dark blue color is related to the low and the red to the higher velocities.

Results

Table 1 shows a selected sample of the primary tracing, and the correspondent multiple for all CMPs, as a result of applying the method based on equation (7). These observed traveltimes are the ones necessary to obtain the WH filter coefficients for the predictive deconvolution.

Table 1: Data for the multiple tracing.

CDP	Segment (m)	Primary (s)	Multiple (s)
1-497	1° 0-3317	2.07	4.14
498-713	2° 3317-4750	1.93	3.86
714-919	3° 4750-6120	1.63	3.26
920-1352	4° 6120-9000	1.21	2.42
1353-1989	5° 9000-13244	0.80	1.60
1990-2491	6° 13244-16583	0.42	0.84
2492-2575	7° 16583-17129	0.13	0.34
2576-4628	8° 17129-30800	0.12	0.26

From Table (1) we can see the periodicity of the normal multiple with respect to the primary, what makes possible the application of WH filtering after the NMO correction, but taking in consideration the pulse stretch.

Figure 6 shows the CMPs 400 (above), the 450 (below), the 500 (above) e 550 (below), before (left) and after (right) the predictive multiple deconvolution, respectively.

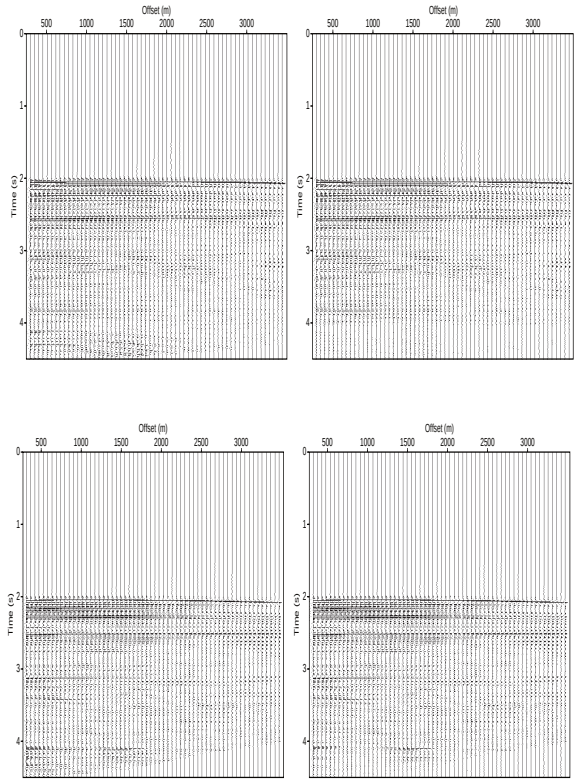

Figure 6: NMO sections CMPs 400 and 450 before and after application of the predictive deconvolution. We can observe the constant periodicity of the multiple, and its attenuation around 4.14s, showing the good result obtained form the deconvolution process. Parameters: *minlag*=2.07s e *maxlag*=4.14s obtained from the multiple tracing experiment.

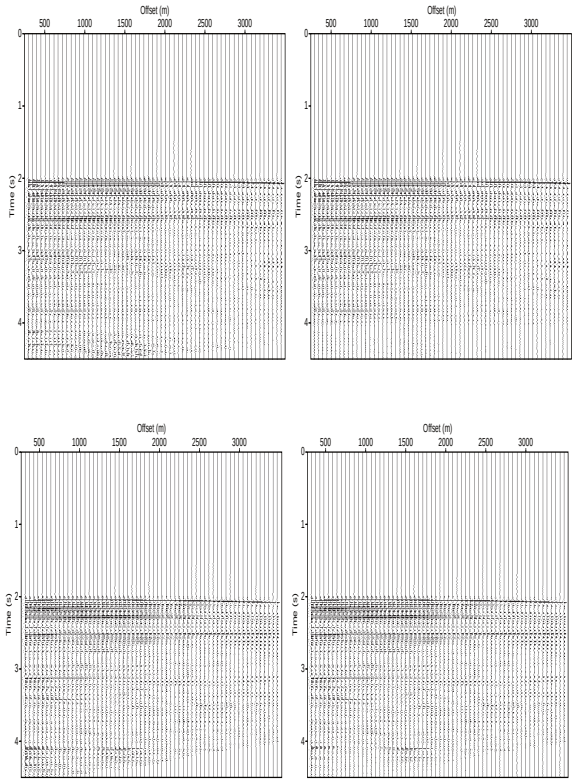

Figure 7: NMO section, CMPs 400 and 450 before and after the application of the multiple predictive deconvolution. We observe the constant periodicity of the multiple reflection, and its attenuation around 4.14s, showing the good result obtained from the deconvolution process. Parameters: *minlag*=2.07s and *maxlag*=4.14s obtained from the tracing experiment.

Figures 6 and 7 show CMPs 400 (above) and 450 (below), before (left) and after (right) the predictive multiple deconvolution, respectively.

Figure 8 shows the stack section after the application of the WH deconvolution. In this figure we observe typical characteristics of diffraction events, and from specular reflections, the ocean bottom time contour, as well as the free surface multiple attenuation.

In this work we performed a post-stack time Kirchhoff migration using $v_{\mathrm{RMS}}(t)$ a velocity model shown in Figure 5 obtained from the semblance velocity analysis, where the major coherence reflection events were picked. Analyzing this this section (see Figure 9) we can see that the structures of the subsurface shift a little with respect to to stack section of Figure 8. An advantage of this section is that we can identify structures a little realized in the stack section minimum offset, and as a result we can see better reflector continuity.

The time migration section obtained in this work is shown also in Figure 9.

The RMS time velocity model was converted to depth using Dix-Durbaum transform to interval velocity, and the result is shown in Figure 10.

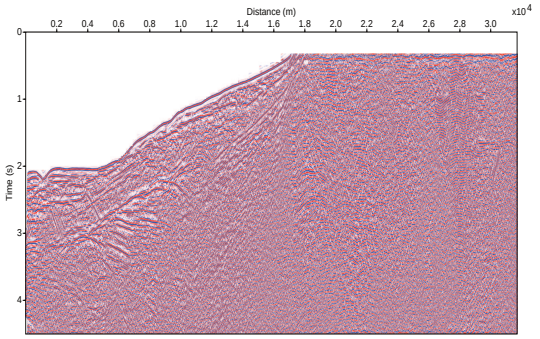

Figure 8: NMO stack section of Camamu line L5519 using manual picking in the semblance map, where we can see that the major part of the registered information corresponds to shallow events, and the reflections have good trace-to-trace correlation giving good continuity. We also observe the multiple attenuation in the inferior left part of the section around 4.14s, and showing that the deconvolution experiment gave satisfactory results.

We have also converted the time stack section to depth by a change of scale of the time axis, where the the stack velocity has been previously resampled form time to depth, as shown in Figure 10. The time stack to depth stack is

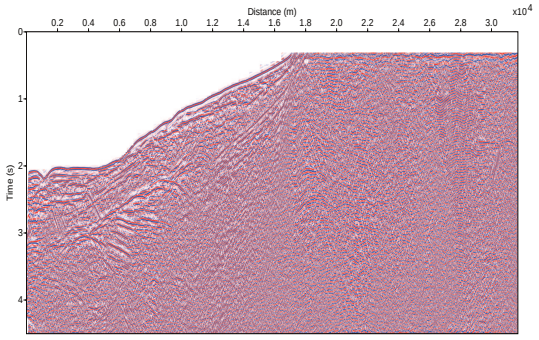

Figure 9: Post stack time Kirchhoff migration of Camamu line L5519, form NMO stack section of Figure 8, and using the RMS velocity model of Figure 5. We can observe the partial diffraction collapse, and the recover of reflection events in the deeper time part of the section. But, we observe arc structures over the diffraction points in the deeper time parts of the section.

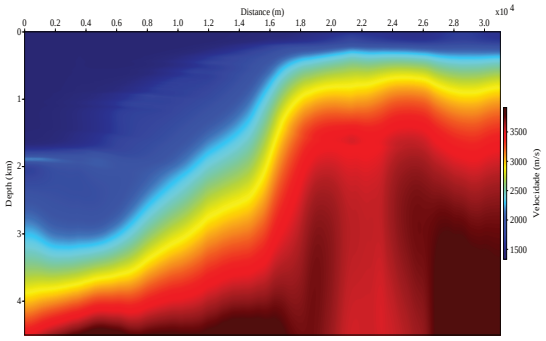

Figure 10: Depth velocity distribution map of Camamu line L5519 obtained from Figure 5 by conversion of $v_{\text{rms}}(t)$ to $v_{\text{int}}(z)$ velocity.

shown in fig. 11.

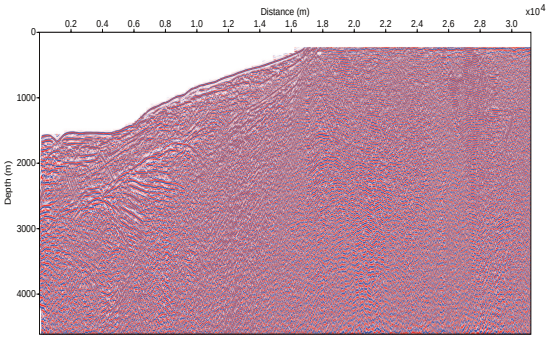

Figure 11: NMO stack (see Figure 8) of Camamu line L5519 rescaled to depth using the velocity model of Figure 10,using a linear interpolation and a constant extrapolation on the semblance map to determine the $v_{\text{int}}(z)$ velocities for non specified intervals. Observe that the section was rescaled only to the depth of 4612m.

Figure 12 shows the depth migration section, where we observe the diffraction collapse, as well as the recovering of several reflection events showing a better result than the time migration.

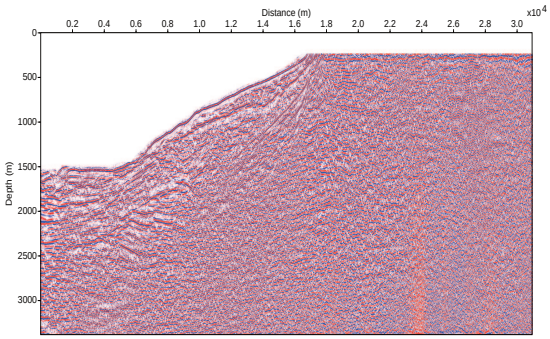

Figure 12: Kirchhoff depth migration of Camamu line L5519 from the NMO stack section (see Figure 8) using the velocity model of Figure 10. We see the recovering of subhorizontal structures traced by the better continuity of reflection events, the diffraction collapse, lineament as geological faulting, the recovering of several reflectors at deeper time part of the section, and the absence of arcs over the diffraction points ("smile types), existent in the migration of Figure 9. Due to further geological information, the considered depth was 3.380m. The migration aperture parameter was taken as 300m.

Conclusions

The WH operator for the case of predictive multiple deconvolution in time domain was designed for marine seismic sections, where the periodicity parameter needs strong a priori information about the topography of the sea continental platform, from where we trace the primary and the multiple, according to the Normal or Oblique case.

The operator was designed to predict the multiple, and the results shown in Figs. 6 e 7.

The velocity analysis was performed in the semblance map for reflection events on 92 CDPs, from a total of 4628 CDPs. The obtained velocity model is presented in Figure 5, where we observe the structure of the continental slope.

The multiple attenuation was performed on the data after the NMO correction, once the events were flattened, and the results can be seen in Figs. 6 and 7, where we can see the multiple attenuation in sections of CMP 400, 450, 500 and 550. We observe that the filter has a good performance for small offsets, mas less resolution as the offset increases. As a conclusion, we need to review this work looking for an operator that changes the performance wit offset distance, in order to take care of the pulse stretching.

A natural procedure is to perform time stack after deconvolution, and the result is present in Figure 8. We observe a meaningful increase in the S/N ratio, where the shallow events are highlighted, and the free surface multiple attenuation acts in the 4s window.

A post-stack time Kirchhoff migration shown in Figure 9, that was obtained from the stack section of Figure 8, using the velocity model of Figure 5. the conclusion was for the partial collapse of some diffraction events, and the recovering of depth reflection events. But, still undesirable

arc shape events are present in the deeper parts of the section.

A time-to-depth conversion was done using the RMS time velocity distribution of Figure 5 (interval velocity) of Figure 10.

Also, a scale change of time-to-depth for the NMO stack of Figure 8. For this, it was used the interval velocity model of Figure 10 from a linear interpolation, and a constant extrapolation for points picked in the semblance map to determine the $v_{\text{int}}(z)$ velocities for non specified time intervals. In this case the section was rescaled to 4612m depth.

The post-stack Kirchhoff depth migration (Figure 12) was performed from the NMO stack section of Figure 8 using the in depth interval velocity model from Figure 10. in this migration we observe: the recovering of subhorizontal structures indicated by the better continuity of the reflection events; the collapse of diffractions; a correction over the interpreted geological faulting; the recovering of several reflectors in depth; the absence of arc-effects over the diffraction points existent in the Kirchhoff time migration of Figure 9. The geological section was scaled to 3300m. For the migration process we have tested several apertures: 200, 300, 400, and 500m, where we observed that with the increase of the aperture, the quantity of artifacts rapidly increases, and the best result is for around 300m.

References

Berkhout, A. J., and Zaanen, P. R., 1979, A comparison between wiener filtering, kalman filtering and deterministic least squares estimation: Geophysical Prospecting, **24**, no. 3, 141–197.

Carneiro, R. N. S., 2012, Marcação e atenuação de múltiplas de superfície livre, processamento e imageamento em dados sísmicos marinhos: Master's thesis, Universidade Federal do Pará.

Cohen, J. K., and Stockwell, J. J. W., 2005, Seismic un*x release n. 39: Center for Wave Phenomena, Colorado School of Mines.

Forel, D., Benz, T., and Pennington, W. D., 2005, Seismic data processing with seismic un*x - a 2d seismic data processing primer: Society of Exploration Geophysicists.

Makhoul, J., 1978, Linear prediction: a tutorial review:, pages 99–118.

Mesko, A., 1984, Digital filtering: Application in geophysical exploration for oil: Pittman Advanced Publishing Program.

Olhovich, V. A., 1959, Curso de sismologia aplicada: Editorial Reverté, Barcelona, Mexico.

Peacook, K., and Treitel, L., 1969, Predictive deconvolution: Theory and practice: Geophysics, , no. 34, 155–169.

Robinson, E. A., and Treitel, S., 1969, Predictive deconvolution: Theory and practice: Geophysics, **34**, no. 2, 155–169.

Robinson, E., 1984, Seismic inversion and deconvolution: Geophysical Press. London.

Acknowledgments

The authors would like to thank the sponsorship of the Project INCT-GP. And in special to the Project PRH-06 that is present in part of this research aiming at oil and gas exploration. We extend our thanks also to the Project FINEP-Fase-5, and to CAPES for the scholarship.